Science Advances
AAAS

Supplementary Materials for

Early sea ice decline off East Antarctica at the last glacial–interglacial climate transition

Henrik Sadatzki *et al.*

Corresponding author: Henrik Sadatzki, hsadatzki@marum.de

Sci. Adv. **9**, eadh9513 (2023)
DOI: 10.1126/sciadv.adh9513

The PDF file includes:

Other Supplementary Material for this manuscript includes the following:

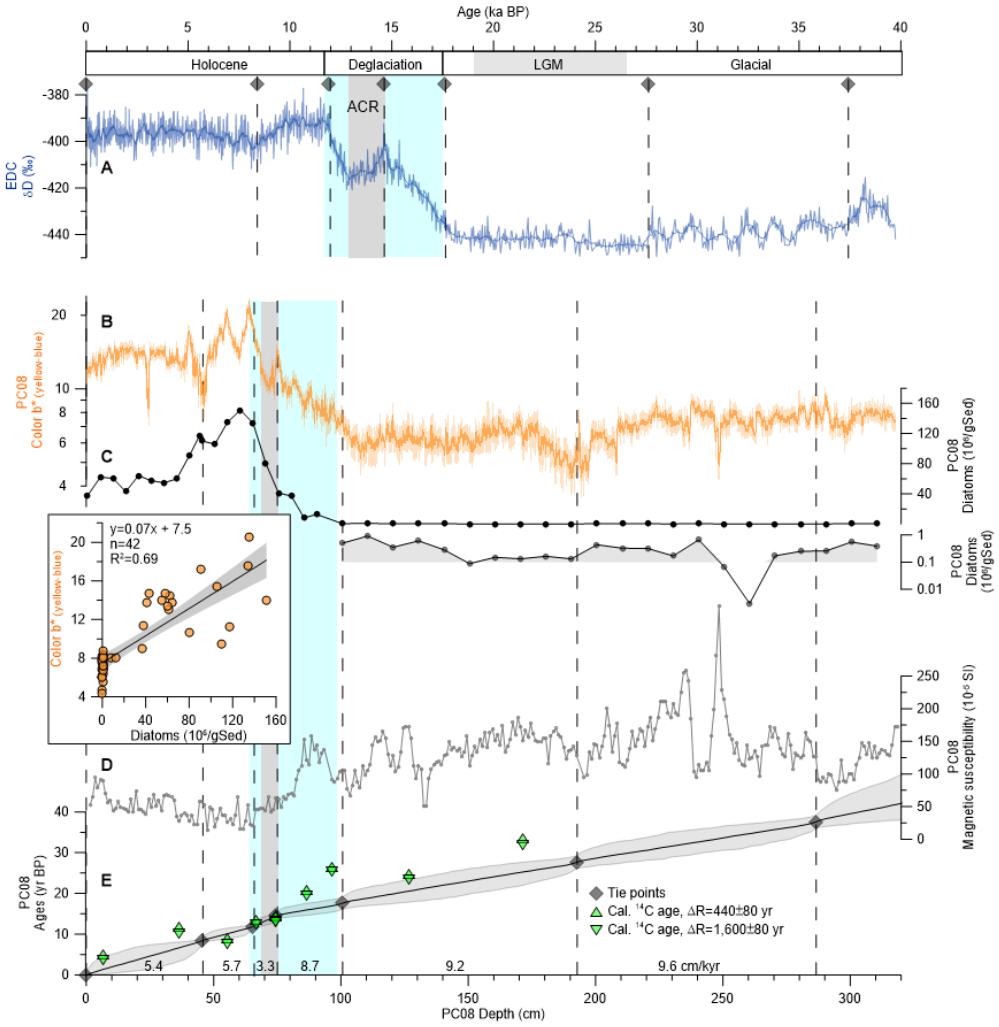

Fig. S1.

Chronology of core PC08 for the last 40 thousand years. (**A**) δD of the EDC ice core with the thick line showing the 15-point running average (*3*) (blue). (**B**) Color b* with the thick line showing the 15-point running average (orange). (**C**) Total diatom abundance (black), for the glacial also plotted on a logarithmic scale (gray). A cross-plot reveals a positive correlation between color b* and total diatom abundance data, where the black line and gray shading indicate the linear regression and its 95% confidence interval. (**D**) Magnetic susceptibility (gray). (**E**) Calibrated acid insoluble organic matter (AIOM) ^{14}C ages using the MARINE20 calibration curve (*80*) and an additional reservoir age correction of either ΔR^{Hol} = 440±80 yr or ΔR^{CS} = 1,600±80 yr (green triangles, table S1); Tuning-based chronology with its 50% quantile (median ages, black line) as well as 2.5% and 97.5% quantiles (gray shading) based on seven age-depth tie points (gray diamonds, table S2). The record in **A** is plotted on the AICC2012 chronology (*30*) and records in **B**–**E** are plotted versus PC08 core depth. Gray diamonds at the top and vertical gray dashed lines mark tie points used for the chronology of PC08 (table S2). Calculated sedimentation rates for the intervals between the tie points are given at the bottom (table S2). Gray shading at the top indicates the Last Glacial Maximum (LGM) after Clark *et al.* (*93*). Light cyan shadings indicate phases of deglacial Antarctic warming and the gray bar marks the Antarctic Cold Reversal (ACR).

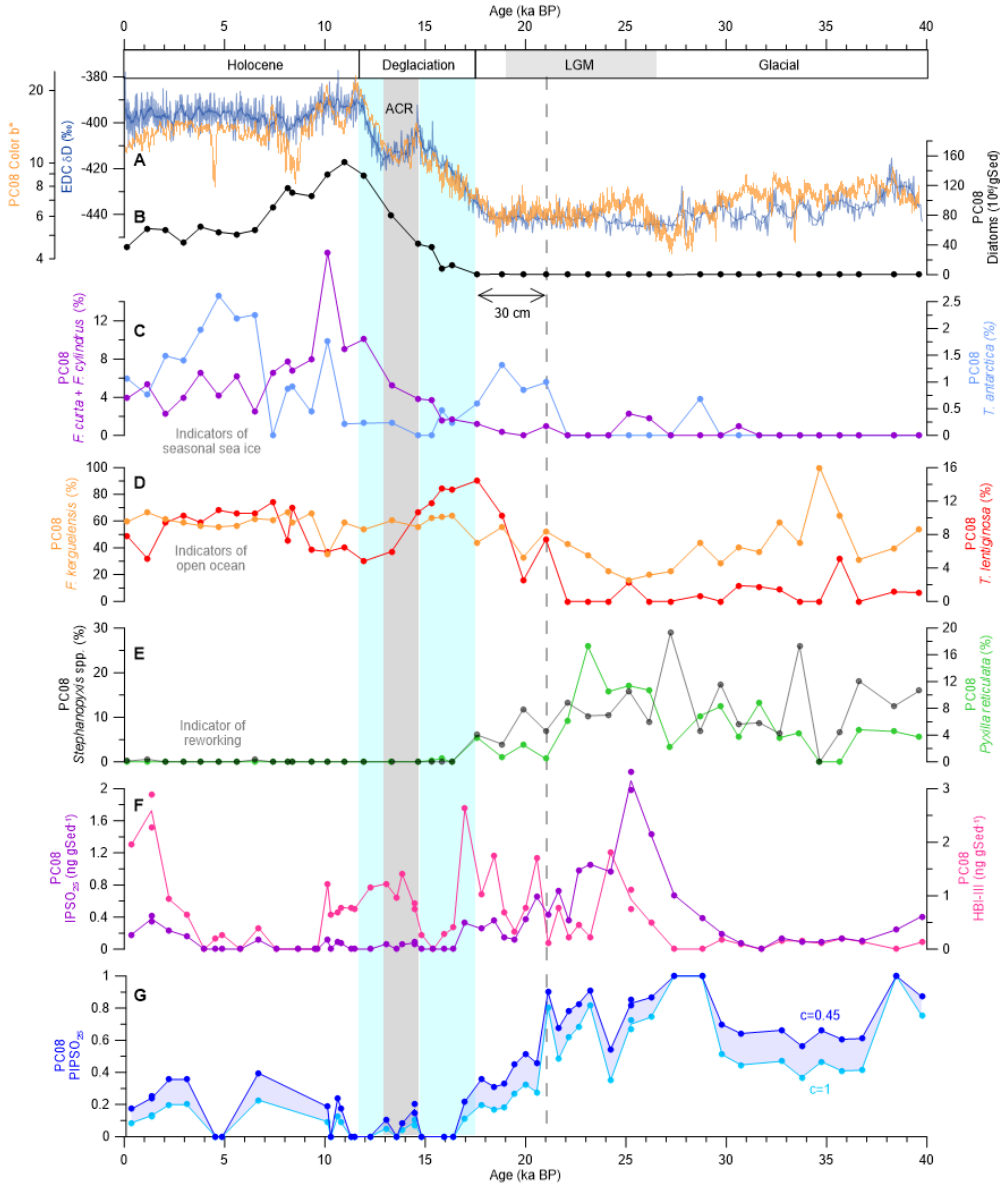

Fig. S2.

Diatom abundance records of core PC08. (**A**) Color b* plotted as 15-point running average (orange) and δD of the EDC ice core with the thick line showing the 15-point running average (*3*, *30*) (blue). (**B**) Total diatom abundance (black). (**C**) *Fragilariopsis curta* plus *Fragilariopsis cylindrus* (purple) and *Thalassiosira antarctica* (light blue). (**D**) *Fragilariopsis kerguelensis* (orange) and *Thalassiosira lentiginosa* (red). (**E**) *Stephanopyxis* spp. and *Pyxilla reticulata* (green). (**F**) $IPSO_{25}$ (purple) and HBI-III (pink). (**G**) $PIPSO_{25}$ (dark blue for c=0.45, light blue for c=1), reflecting sea ice conditions. The vertical gray dashed line marks the point at which diatom and biomarker data suggest a first breakup of the glacial sea ice cover, 30 cm below the point defined as the onset of the deglaciation. Gray shading at the top indicates the Last Glacial Maximum (LGM) after Clark *et al.* (*93*). Light cyan shadings indicate phases of deglacial Antarctic warming and the gray bar marks the Antarctic Cold Reversal (ACR).

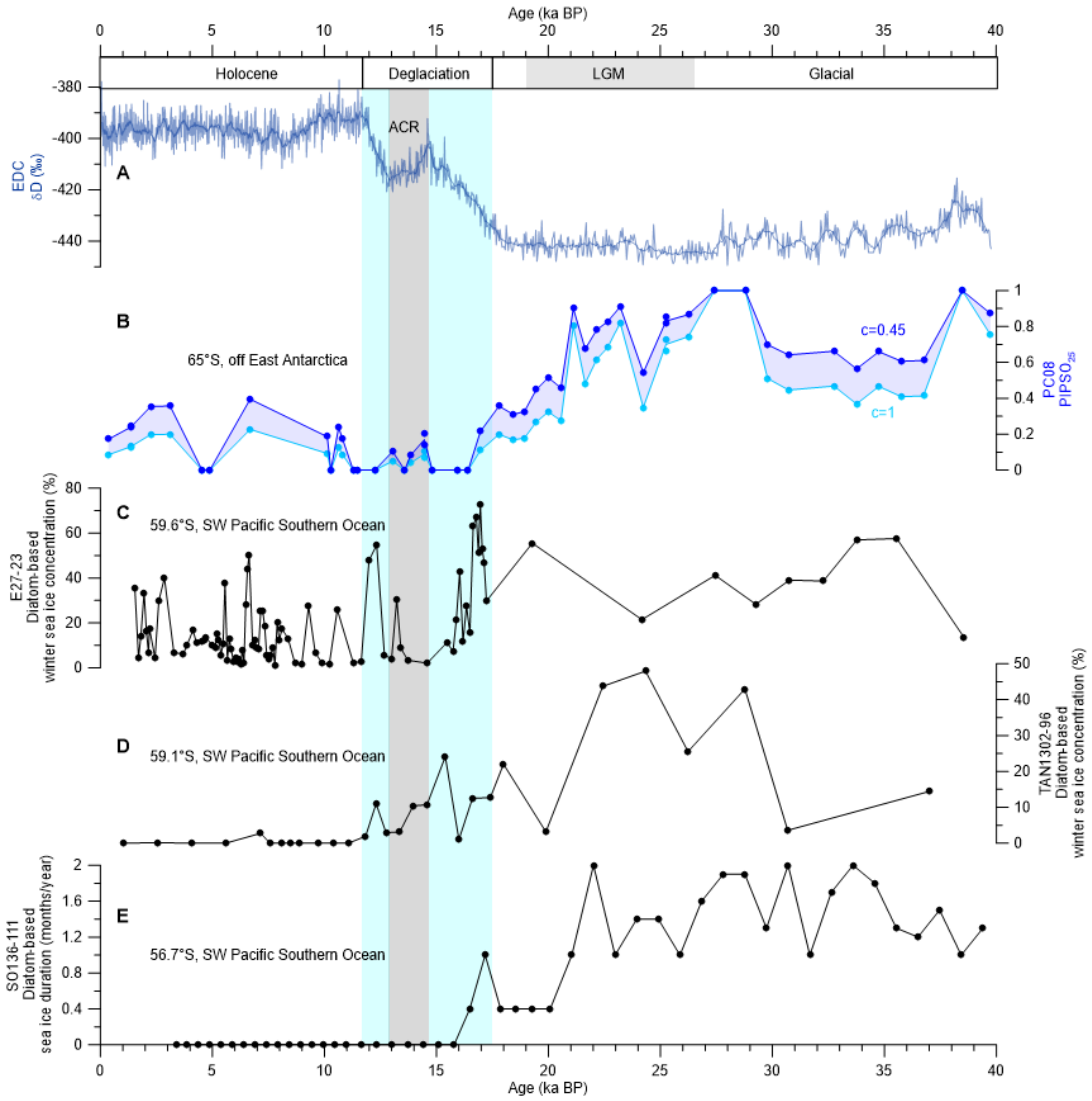

Fig. S3.

Sea ice records based on biomarkers and diatoms. (**A**) δD of the EDC ice core with the thick line showing the 15-point running average (*3*, *30*). (**B**) $PIPSO_{25}$ of core PC08 (dark blue for c=0.45, light blue for c=1). (**C**) Diatom-based winter sea ice concentration record of core E27-23 (*43*). (**D**) Diatom-based sea ice concentration record of core TAN1302-96 (*22*). (**E**) Diatom-based sea ice duration record of core SO136-111 (*45*). Gray shading at the top indicates the Last Glacial Maximum (LGM) after Clark *et al.* (*93*). Light cyan shadings indicate phases of deglacial Antarctic warming and the gray bar marks the Antarctic Cold Reversal (ACR).

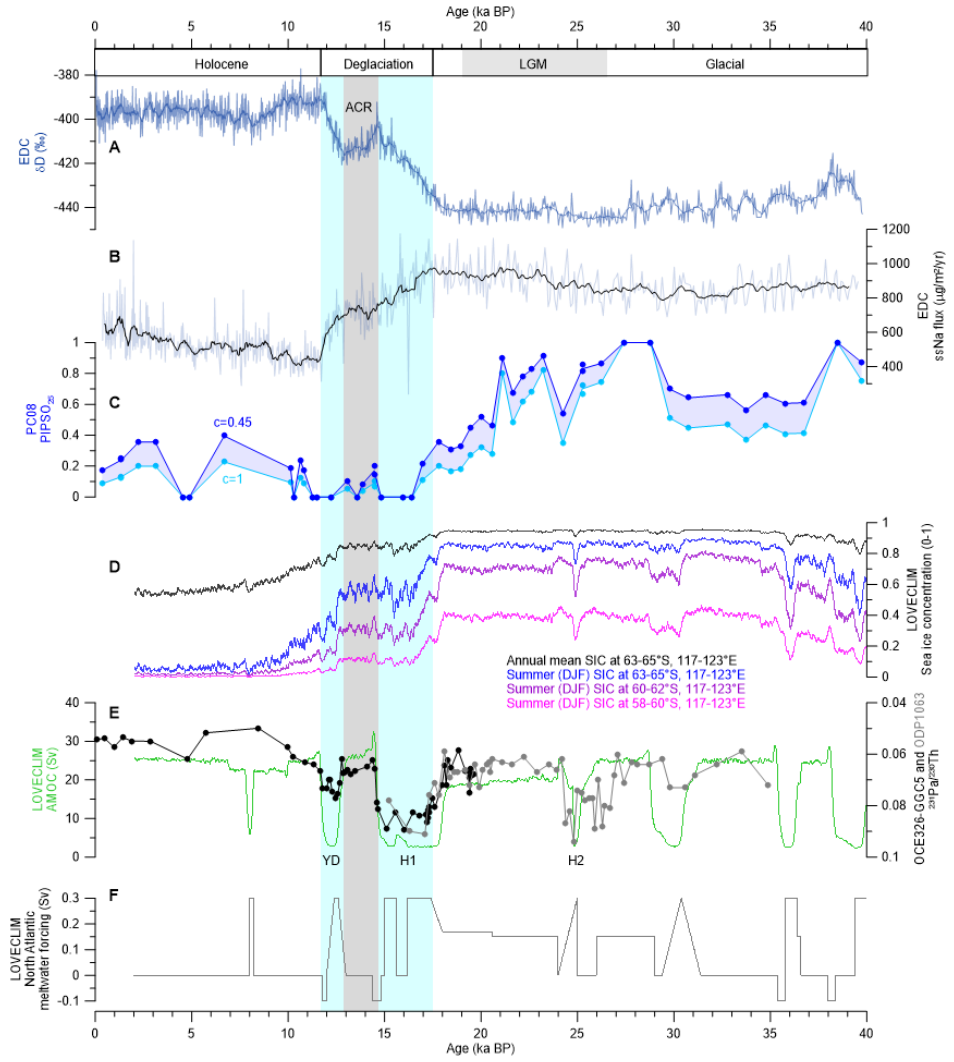

Fig. S4.

Proxy-model data comparison. (**A**) δD of the EDC ice core with the thick line showing the 15-point running average (*3, 30*). (**B**) Sea salt sodium (ssNa) flux of the EDC ice core with the thick line showing the 15-point running average (*52*). (**C**) $PIPSO_{25}$ of core PC08 (dark blue for c=0.45, light blue for c=1). (**D**) Simulated annual mean sea ice concentration (black) and summer (Dec-Jan-Feb) sea ice concentration for core site PC08 (blue) averaged over 63°S–65°S, 117°E–123°E, and summer (Dec-Jan-Feb) sea ice concentration north of core site PC08 averaged over 60°S–62°S, 117°E–123°E (purple) and averaged over 58°S–60°S, 117°E–123°E (magenta), plotted as 101-year running averages (*18, 24*). (**E**) Simulated Atlantic Meridional Overturning Circulation (AMOC) plotted as 101-year running averages (*18, 24*) (green) and sedimentary $^{231}Pa/^{230}Th$ records of cores OCE326-GGC5 (*14*) (black) and ODP1063 (*100*) (gray). (**F**) North Atlantic meltwater forcing of the transient model simulation (*18, 24*). Gray shading at the top indicates the Last Glacial Maximum (LGM) after Clark *et al.* (*93*). Light cyan shadings indicate phases of deglacial Antarctic warming, concurrent with major reductions in the $^{231}Pa/^{230}Th$–based AMOC associated with Heinrich Stadial 1 (H1) and the Younger Dryas (YD), and the gray bar marks the Antarctic Cold Reversal (ACR). The AMOC reduction associated with Heinrich Stadial 2 (H2) is also marked at the bottom.

Table S1.

Acid insoluble organic matter (AIOM) ^{14}C ages in core PC08. AIOM ^{14}C ages were calibrated using Calib 8.20 (*79*), the MARINE20 calibration curve (*80*), and two different additional reservoir age correction (ΔR) scenarios following recommendations by Heaton *et al.* (*81*). Calibrated ^{14}C ages shown are based on the 1σ range and median probability (bold in brackets).

Core depth cm	Lab ID	AIOM ^{14}C age ± SD yr BP	Cal. ^{14}C age (for ΔR^{Hol}=440±80 yr) yr BP	Cal. ^{14}C age (for ΔR^{CS}=1,600±80 yr) yr BP
6.50	SANU-64333	5,382 ± 28	4,919–5,200 (**5,055**)	3,431–3,679 (**3,553**)
36.50	SANU-64335	11,096 ± 35	11,634–11,974 (**11,812**)	10,041–10,324 (**10,183**)
55.50	SANU-64336	8,894 ± 30	8,706–8,988 (**8,844**)	7,476–7,674 (**7,581**)
66.50	SANU-64337	12,667 ± 41	13,451–13,704 (**13,572**)	12,295–12,585 (**12,420**)
74.50	SANU-64404	13,381 ± 41	14,427–14,838 (**14,624**)	12,991–13,222 (**13,103**)
74.50	SANU-64411	13,161 ± 41	14,042–14,413 (**14,244**)	12,766–12,988 (**12,888**)
86.50	SANU-64405	18,350 ± 62	20,542–20,850 (**20,701**)	19,142–19,466 (**19,303**)
96.50	SANU-64406	23,466 ± 101	26,159–26,597 (**26,385**)	25,085–25,458 (**25,266**)
126.50	SANU-64407	21,863 ± 81	24,576–24,947 (**24,755**)	23,271–23,642 (**23,433**)
171.50	SANU-64409	30,147 ± 197	33,108–33,656 (**33,377**)	31,464–32,029 (**31,765**)

Table S2.

Age-depth tie points and sedimentation rates of core PC08 for the interval 0–40 ka. EDC ages and age uncertainties are based on the AICC2012 chronology (*30*).

PC08 Core depth cm	EDC $Age_{AICC2012}$ ka BP	EDC $Age_{AICC2012}$ uncertainty kyr	Sedimentation rate cm/kyr
0.00	0.0	0.1	
45.50	8.4	0.2	5.4
65.50	11.9	0.3	5.7
74.50	14.6	0.4	3.3
100.50	17.6	0.8	8.7
192.50	27.6	0.8	9.2
286.50	37.4	0.8	9.6

Data S1. (separate file)

Magnetic susceptibility and b* color data from core IN2017_V01_C025_PC08, covering 0–40 ka BP.

Data S2. (separate file)

Diatom data (total diatom abundance and relative abundances of *F. curta*, *F. cylindrus*, *T. antarctica*, *F. kerguelensis*, *T. lentiginosa*, *Stephanopyxis* spp., *Pyxilla reticulata*) from core IN2017_V01_C025_PC08, covering 0–40 ka BP.

Data S3. (separate file)

HBI biomarker data ($IPSO_{25}$, HBI-III, $IPSO_{25}$/HBI-III, $PIPSO_{25}$) from core IN2017_V01_C025_PC08, covering 0–40 ka BP.

Data S4. (separate file)

Model output data (simulated Antarctic sea ice concentration and Atlantic Meridional Overturning Circulation) and North Atlantic meltwater forcing of a transient experiment with the Earth system model LOVECLIM, covering 0–40 ka BP.

REFERENCES AND NOTES

1. E. Monnin, A. Indermühle, A. Dällenbach, J. Flückiger, B. Stauffer, T. F. Stocker, D. Raynaud, J.-M. Barnola, Atmospheric CO_2 concentrations over the last glacial termination. *Science* **291**, 112–114 (2001).

2. F. Parrenin, V. Masson-Delmotte, P. Köhler, D. Raynaud, D. Paillard, J. Schwander, C. Barbante, A. Landais, A. Wegner, J. Jouzel, Synchronous change of atmospheric CO_2 and Antarctic temperature during the last deglacial warming. *Science* **339**, 1060–1063 (2013).

3. J. Jouzel, V. Masson-Delmotte, O. Cattani, G. Dreyfus, S. Falourd, G. Hoffmann, B. Minster, J. Nouet, J. M. Barnola, J. Chappellaz, H. Fischer, J. C. Gallet, S. Johnsen, M. Leuenberger, L. Loulergue, D. Luethi, H. Oerter, F. Parrenin, G. Raisbeck, D. Raynaud, A. Schilt, J. Schwander, E. Selmo, R. Souchez, R. Spahni, B. Stauffer, J. P. Steffensen, B. Stenni, T. F. Stocker, J. L. Tison, M. Werner, E. W. Wolff, Orbital and millennial Antarctic climate variability over the past 800,000 years. *Science* **317**, 793–796 (2007).

4. C. Basak, H. Fröllje, F. Lamy, R. Gersonde, V. Benz, R. F. Anderson, M. Molina-Kescher, K. Pahnke, Breakup of last glacial deep stratification in the South Pacific. *Science* **359**, 900–904 (2018).

5. L. C. Skinner, S. Fallon, C. Waelbroeck, E. Michel, S. Barker, Ventilation of the deep Southern Ocean and deglacial CO_2 rise. *Science* **328**, 1147–1151 (2010).

6. R. F. Anderson, S. Ali, L. I. Bradtmiller, S. H. H. Nielsen, M. Q. Fleisher, B. E. Anderson, L. H. Burckle, Wind-driven upwelling in the Southern Ocean and the deglacial rise in atmospheric CO_2. *Science* **323**, 1443–1448 (2009).

7. G. H. Denton, R. F. Anderson, J. R. Toggweiler, R. L. Edwards, J. M. Schaefer, A. E. Putnam, The last glacial termination. *Science* **328**, 1652–1656 (2010).

8. D. J. Wilson, T. Struve, T. van de Flierdt, T. Chen, T. Li, A. Burke, L. F. Robinson, Sea-ice control on deglacial lower cell circulation changes recorded by Drake Passage deep-sea corals. *Earth Planet. Sci. Lett.* **544**, 116405 (2020).

9. R. Ferrari, M. F. Jansen, J. F. Adkins, A. Burke, A. L. Stewart, A. F. Thompson, Antarctic sea ice control on ocean circulation in present and glacial climates. *Proc. Natl. Acad. Sci. U.S.A.* **111**, 8753–8758 (2014).

10. L.-P. Nadeau, R. Ferrari, M. F. Jansen, Antarctic sea ice control on the depth of North Atlantic deep water. *J. Climate* **32**, 2537–2551 (2019).

11. B. B. Stephens, R. F. Keeling, The influence of Antarctic sea ice on glacial-interglacial CO_2 variations. *Nature* **404**, 171–174 (2000).

12. S. Barker, P. Diz, M. J. Vautravers, J. Pike, G. Knorr, I. R. Hall, W. S. Broecker, Interhemispheric Atlantic seesaw response during the last deglaciation. *Nature* **457**, 1097–1102 (2009).

13. S. O. Rasmussen, M. Bigler, S. P. Blockley, T. Blunier, S. L. Buchardt, H. B. Clausen, I. Cvijanovic, D. Dahl-Jensen, S. J. Johnsen, H. Fischer, V. Gkinis, M. Guillevic, W. Z. Hoek, J. J. Lowe, J. B. Pedro, T. Popp, I. K. Seierstad, J. P. Steffensen, A. M. Svensson, P. Vallelonga, B. M. Vinther, M. J. C. Walker, J. J. Wheatley, M. Winstrup, A stratigraphic framework for abrupt climatic changes during the Last Glacial period based on three synchronized Greenland ice-core records: Refining and extending the INTIMATE event stratigraphy. *Quat. Sci. Rev.* **106**, 14–28 (2014).

14. J. F. McManus, R. Francois, J. M. Gherardi, L. D. Keigwin, S. Brown-Leger, Collapse and rapid resumption of Atlantic meridional circulation linked to deglacial climate changes. *Nature* **428**, 834–837 (2004).

15. T. F. Stocker, S. J. Johnsen, A minimum thermodynamic model for the bipolar seesaw. *Paleoceanography* **18**, 1087 (2003).

16. J. Gottschalk, G. Battaglia, H. Fischer, T. L. Frölicher, S. L. Jaccard, A. Jeltsch-Thömmes, F. Joos, P. Köhler, K. J. Meissner, L. Menviel, C. Nehrbass-Ahles, J. Schmitt, A. Schmittner, L. C. Skinner, T. F. Stocker, Mechanisms of millennial-scale atmospheric CO_2 change in numerical model simulations. *Quat. Sci. Rev.* **220**, 30–74 (2019).

17. J. B. Pedro, H. C. Bostock, C. M. Bitz, F. He, M. J. Vandergoes, E. J. Steig, B. M. Chase, C. E. Krause, S. O. Rasmussen, B. R. Markle, G. Cortese, The spatial extent and dynamics of the Antarctic Cold Reversal. *Nat. Geosci.* **9**, 51–55 (2016).

18. L. Menviel, A. Timmermann, O. E. Timm, A. Mouchet, Deconstructing the Last Glacial termination: The role of millennial and orbital-scale forcings. *Quat. Sci. Rev.* **30**, 1155–1172 (2011).

19. WAIS Divide Project Members, Onset of deglacial warming in West Antarctica driven by local orbital forcing. *Nature* **500**, 440–444 (2013).

20. T. A. Ronge, J. Lippold, W. Geibert, S. L. Jaccard, S. Mieruch-Schnülle, F. Süfke, R. Tiedemann, Deglacial patterns of South Pacific overturning inferred from ^{231}Pa and ^{230}Th. *Sci. Rep.* **11**, 20473 (2021).

21. X. Crosta, K. E. Kohfeld, H. C. Bostock, M. Chadwick, A. Du Vivier, O. Esper, J. Etourneau, J. Jones, A. Leventer, J. Müller, R. H. Rhodes, C. S. Allen, P. Ghadi, N. Lamping, C. B. Lange, K.-A. Lawler, D. Lund, A. Marzocchi, K. J. Meissner, L. Menviel, A. Nair, M. Patterson, J. Pike, J. G. Prebble, C. Riesselman, H. Sadatzki, L. C. Sime, S. K. Shukla, L. Thöle, M.-E. Vorrath, W. Xiao, J. Yang, Antarctic sea ice over the past 130,000 years—Part 1: A review of what proxy records tell us. *Clim. Past* **18**, 1729–1756 (2022).

22. M. Chadwick, X. Crosta, O. Esper, L. Thöle, K. E. Kohfeld, Compilation of Southern Ocean sea-ice records covering the last glacial-interglacial cycle (12–130 ka). *Clim. Past* **18**, 1815–1829 (2022).

23. R. Gersonde, U. Zielinski, The reconstruction of late Quaternary Antarctic sea-ice distribution—The use of diatoms as a proxy for sea-ice. *Palaeogeogr. Palaeoclimatol. Palaeoecol.* **162**, 263–286 (2000).

24. L. Menviel, A. Timmermann, T. Friedrich, M. H. England, Hindcasting the continuum of Dansgaard-Oeschger variability: Mechanisms, patterns and timing. *Clim. Past* **10**, 63–77 (2014).

25. L. K. Armand, P. E. O'Brien, On-board Scientific Party, Interactions of the Totten Glacier with the Southern Ocean through multiple glacial cycles (IN2017-V01): Post-survey report. Research School of Earth Sciences, Australian National University, Canberra, https://doi.org/10.4225/13/5acea64c48693 (2018).

26. T. Tamura, K. I. Ohshima, S. Nihashi, Mapping of sea ice production for Antarctic coastal polynyas. *Geophys. Res. Lett.* **35**, L07606 (2008).

27. L. Holder, M. Duffy, B. Opdyke, A. Leventer, A. Post, P. O'Brien, L. K. Armand, Controls since the mid-Pleistocene transition on sedimentation and primary productivity downslope of Totten Glacier, East Antarctica. *Paleoceanogr. Paleoclimatol.* **35**, e2020PA003981 (2020).

28. S. Tooze, J. A. Halpin, T. L. Noble, Z. Chase, P. E. O'Brien, L. Armand, Scratching the surface: A marine sediment provenance record from the continental slope of central Wilkes Land, East Antarctica. *Geochem. Geophys. Geosyst.* **21**, e2020GC009156 (2020).

29. D. Sprenk, M. E. Weber, G. Kuhn, P. Rosén, M. Frank, M. Molina-Kescher, V. Liebetrau, H.-G. Röhling, Southern Ocean bioproductivity during the last glacial cycle—New detection method and decadal-scale insight from the Scotia Sea. *Geol. Soc. Lond. Spec. Publ.* **381**, 245–261 (2013).

30. D. Veres, L. Bazin, A. Landais, H. T. M. Kele, B. Lemieux-Dudon, F. Parrenin, P. Martinerie, E. Blayo, T. Blunier, E. Capron, J. Chappellaz, S. O. Rasmussen, M. Severi, A. Svensson, B. Vinther, E. W. Wolff, The Antarctic ice core chronology (AICC2012): An optimized multi-parameter and multi-site dating approach for the last 120 thousand years. *Clim. Past* **9**, 1733–1748 (2013).

31. J. Fenner, Eocene-Oligocene planktic diatom stratigraphy in the low latitudes and the high southern latitudes. *Micropaleontology* **30**, 319–342 (1984).

32. P. E. O'Brien, A. L. Post, S. Edwards, T. Martin, A. Caburlotto, F. Donda, G. Leitchenkov, R. Romero, M. Duffy, D. Evangelinos, L. Holder, A. Leventer, A. López-Quirós, B. N.

Opdyke, L. K. Armand, Continental slope and rise geomorphology seaward of the Totten Glacier, East Antarctica (112°E-122°E). *Mar. Geol.* **427**, 106221 (2020).

33. G. Massé, S. T. Belt, X. Crosta, S. Schmidt, I. Snape, D. N. Thomas, S. J. Rowland, Highly branched isoprenoids as proxies for variable sea ice conditions in the Southern Ocean. *Antarct. Sci.* **23**, 487–498 (2011).

34. S. T. Belt, L. Smik, T. A. Brown, J.-H. Kim, S. J. Rowland, C. S. Allen, J.-K. Gal, K.-H. Shin, J. I. Lee, K. W. R. Taylor, Source identification and distribution reveals the potential of the geochemical Antarctic sea ice proxy $IPSO_{25}$. *Nat. Commun.* **7**, 12655 (2016).

35. S. T. Belt, Source-specific biomarkers as proxies for Arctic and Antarctic sea ice. *Org. Geochem.* **125**, 277–298 (2018).

36. L. Smik, S. T. Belt, J. L. Lieser, L. K. Armand, A. Leventer, Distributions of highly branched isoprenoid alkenes and other algal lipids in surface waters from East Antarctica: Further insights for biomarker-based paleo sea-ice reconstruction. *Org. Geochem.* **95**, 71–80 (2016).

37. M.-E. Vorrath, J. Müller, O. Esper, G. Mollenhauer, C. Haas, E. Schefuß, K. Fahl, Highly branched isoprenoids for Southern Ocean sea ice reconstructions: A pilot study from the Western Antarctic Peninsula. *Biogeosciences*, **16**, 2961–2981 (2019).

38. J. Müller, A. Wagner, K. Fahl, R. Stein, M. Prange, G. Lohmann, Towards quantitative sea ice reconstructions in the northern North Atlantic: A combined biomarker and numerical modelling approach. *Earth Planet. Sci. Lett.* **306**, 137–148 (2011).

39. N. Lamping, J. Müller, J. Hefter, G. Mollenhauer, C. Haas, X. Shi, M.-E. Vorrath, G. Lohmann, C.-D. Hillenbrand, Evaluation of lipid biomarkers as proxies for sea ice and ocean temperatures along the Antarctic continental margin. *Clim. Past* **17**, 2305–2326, (2021).

40. L. K. Armand, X. Crosta, O. Romero, J.-J. Pichon, The biogeography of major diatom taxa in Southern Ocean sediments: 1. Sea ice related species. *Palaeogeogr. Palaeoclimatol. Palaeoecol.* **223**, 93–126 (2005).

41. X. Crosta, J. Etourneau, L. C. Orme, Q. Dalaiden, P. Campagne, D. Swingedouw, H. Goosse, G. Massé, A. Miettinen, R. M. McKay, R. B. Dunbar, C. Escutia, M. Ikehara, Multi-decadal trends in Antarctic sea-ice extent driven by ENSO–SAM over the last 2,000 years. *Nat. Geosci.* **14**, 156–160 (2021).

42. W. S. Xiao, O. Esper, R. Gersonde, Last Glacial–Holocene climate variability in the Atlantic sector of the Southern Ocean. *Quat. Sci. Rev.* **135**, 115–137 (2016).

43. A. J. Ferry, X. Crosta, P. G. Quilty, D. Fink, W. Howard, L. K. Armand, First records of winter sea ice concentration in the southwest Pacific sector of the Southern Ocean. *Paleoceanography* **30**, 1525–1539 (2015).

44. J. Jones, K. E. Kohfeld, H. Bostock, X. Crosta, M. Liston, G. Dunbar, Z. Chase, A. Leventer, H. Anderson, G. Jacobsen, Sea ice changes in the southwest Pacific sector of the Southern Ocean during the last 140,000 years. *Clim. Past* **18**, 465–483 (2022).

45. X. Crosta, A. Sturm, L. Armand, J.-J. Pichon, Late Quaternary sea ice history in the Indian sector of the Southern Ocean as recorded by diatom assemblages. *Mar. Micropaleontol.* **50**, 209–223 (2004).

46. R. Gersonde, X. Crosta, A. Abelmann, L. Armand, Sea-surface temperature and sea ice distribution of the Southern Ocean at the EPILOG Last Glacial Maximum—A circum-Antarctic view based on siliceous microfossil records. *Quat. Sci. Rev.* **24**, 869–896 (2005).

47. L. G. Collins, J. Pike, C. S. Allen, D. A. Hodgson, High-resolution reconstruction of southwest Atlantic sea-ice and its role in the carbon cycle during marine isotope stages 3 and 2. *Paleoceanography* **27**, PA3217 (2012).

48. C. S. Allen, J. Pike, C. J. Pudsey, Last glacial–interglacial sea-ice cover in the SW Atlantic and its potential role in global deglaciation. *Quat. Sci. Rev.* **30**, 2446–2458 (2011).

49. A. Shemesh, D. Hodell, X. Crosta, S. Kanfoush, C. Charles, T. Guilderson, Sequence of events during the last deglaciation in Southern Ocean sediments and Antarctic ice cores. *Paleoceanography* **17**, 8-1–8-7 (2002).

50. R. A. Green, L. Menviel, K. Meissner, X. Crosta, D. Chandan, G. Lohmann, W. R. Peltier, X. Shi, J. Zhu, Evaluating seasonal sea-ice cover over the Southern Ocean at the Last Glacial Maximum. *Clim. Past* **18**, 845–862 (2022).

51. E. W. Wolff, H. Fischer, F. Fundel, U. Ruth, B. Twarloh, G. C. Littot, R. Mulvaney, R. Röthlisberger, M. de Angelis, C. F. Boutron, M. Hansson, U. Jonsell, M. A. Hutterli, F. Lambert, P. Kaufmann, B. Stauffer, T. F. Stocker, J. P. Steffensen, M. Bigler, M. L. Siggaard-Andersen, R. Udisti, S. Becagli, E. Castellano, M. Severi, D. Wagenbach, C. Barbante, P. Gabrielli, V. Gaspari, Southern Ocean sea-ice extent, productivity and iron flux over the past eight glacial cycles. *Nature* **440**, 491–496 (2006).

52. H. Fischer, F. Fundel, U. Ruth, B. Twarloh, A. Wegner, R. Udisti, S. Becagli, E. Castellano, A. Morganti, M. Severi, E. Wolff, G. Littot, R. Röthlisberger, R. Mulvaney, M. A. Hutterli, P. Kaufmann, U. Federer, F. Lambert, M. Bigler, M. Hansson, U. Jonsell, M. de Angelis, C. Boutron, M.-Louise Siggaard-Andersen, J. P. Steffensen, C. Barbante, V. Gaspari, P. Gabrielli, D. Wagenbach, Reconstruction of millennial changes in dust emission, transport and regional sea ice coverage using the deep EPICA ice cores from the Atlantic and Indian Ocean sector of Antarctica. *Earth Planet. Sci. Lett.* **260**, 340–354 (2007).

53. P. De Deckker, M. Moros, K. Perner, E. Jansen, Influence of the tropics and southern westerlies on glacial interhemispheric asymmetry. *Nat. Geosci.* **5**, 266–269 (2012).

54. P. De Deckker, M. Moros, K. Perner, T. Blanz, L. Wacker, R. Schneider, T. T. Barrows, T. O'Loingsigh, E. Jansen, Climatic evolution in the Australian region over the last 94 ka - spanning human occupancy -, and unveiling the Last Glacial Maximum. *Quat. Sci. Rev.* **249**, 106593 (2020).

55. P. Huybers, G. Denton, Antarctic temperature at orbital timescales controlled by local summer duration. *Nat. Geosci.* **1**, 787–792 (2008).

56. A. Timmermann, O. Timm, L. Stott, L. Menviel, The roles of CO_2 and orbital forcing in driving Southern Hemispheric temperature variations during the last 21 000 yr. *J. Clim.* **22**, 1626–1640 (2009).

57. P. Huybers, Early Pleistocene glacial cycles and the integrated summer insolation forcing. *Science* **313**, 508–511 (2006).

58. G. Ménot, E. Bard, F. Rostek, J. W. H. Weijers, E. C. Hopmans, S. Schouten, J. S. Sinninghe Damsté, Early reactivation of European rivers during the last deglaciation. *Science* **313**, 1623–1625 (2006).

59. V. L. Peck, I. R. Hall, R. Zahn, H. Elderfield, F. Grousset, S. R. Hemming, J. D. Scourse, High resolution evidence for linkages between NW European ice sheet instability and Atlantic meridional overturning circulation. *Earth Planet. Sci. Lett.* **243**, 476–488 (2006).

60. A. D. Moy, W. R. Howard, M. K. Gagan, Late Quaternary palaeoceanography of the Circumpolar Deep Water from the South Tasman Rise. *J. Quat. Sci.* **21**, 763–777 (2006).

61. J. R. Toggweiler, J. L. Russell, S. R. Carson, Midlatitude westerlies, atmospheric CO_2, and climate change during the ice ages. *Paleoceanography* **21**, PA2005 (2006).

62. L. Menviel, P. Spence, J. Yu, M. A. Chamberlain, R. J. Matear, K. J. Meissner, M. H. England, Southern Hemisphere westerlies as a driver of the early deglacial atmospheric CO_2 rise. *Nat. Commun.* **9**, 2503 (2018).

63. L. Lu, X. Zheng, Z. Chen, W. Yan, S. Wu, L.-W. Zheng, X. Wang, Y. Chen, S. Kao, One-to-one coupling between Southern Ocean productivity and Antarctica climate. *Geophys. Res. Lett.* **49**, e2022GL098761 (2022).

64. D. M. Sigman, E. A. Boyle, Glacial/interglacial variations in atmospheric carbon dioxide. *Nature* **407**, 859–869 (2000).

65. T. Li, L. F. Robinson, T. Chen, X. T. Wang, A. Burke, J. W. B. Rae, A. Pegrum-Haram, T. D. J. Knowles, G. Li, J. Chen, H. Chin Ng, M. Prokopenko, G. H. Rowland, A. Samperiz, J. A. Stewart, J. Southon, P. T. Spooner, Rapid shifts in circulation and biogeochemistry of the Southern Ocean during deglacial carbon cycle events. *Sci. Adv.* **6**, eabb3807 (2020).

66. J. Gottschalk, E. Michel, L. M. Thöle, A. S. Studer, A. P. Hasenfratz, N. Schmid, M. Butzin, A. Mazaud, A. Martínez-García, S. Szidat, S. L. Jaccard, Glacial heterogeneity in Southern Ocean carbon storage abated by fast South Indian deglacial carbon release. *Nat. Commun.* **11**, 6192 (2020).

67. J. W. B. Rae, A. Burke, L. F. Robinson, J. F. Adkins, T. Chen, C. Cole, R. Greenop, T. Li, E. F. M. Littley, D. C. Nita, J. A. Stewart, B. J. Taylor, CO_2 storage and release in the deep Southern Ocean on millennial to centennial timescales. *Nature* **562**, 569–573 (2018).

68. J. Schmitt, R. Schneider, J. Elsig, D. Leuenberger, A. Lourantou, J. Chappellaz, P. Köhler, F. Joos, T. F. Stocker, M. Leuenberger, H. Fischer, Carbon isotope constraints on the deglacial CO_2 rise from ice cores. *Science* **336**, 711–714 (2012).

69. T. K. Bauska, D. Baggenstos, E. J. Brook, A. C. Mix, S. A. Marcott, V. V. Petrenko, H. Schaefer, J. P. Severinghaus, J. E. Lee, Carbon isotopes characterize rapid changes in atmospheric carbon dioxide during the last deglaciation. *Proc. Natl. Acad. Sci. U.S.A.* **113**, 3465–3470 (2016).

70. S. A. Marcott, T. K. Bauska, C. Buizert, E. J. Steig, J. L. Rosen, K. M. Cuffey, T. J. Fudge, J. P. Severinghaus, J. Ahn, M. L. Kalk, J. R. McConnell, T. Sowers, K. C. Taylor, J. W. C. White, E. J. Brook, Centennial-scale changes in the global carbon cycle during the last deglaciation. *Nature* **514**, 616–619 (2014).

71. J. P. Warnock, R. P. Scherer, A revised method for determining the absolute abundance of diatoms. *J. Paleolimnol.* **53**, 157–163 (2015).

72. A. O. Cefarelli, M. E. Ferrario, G. O. Almandoz, A. G. Atencio, R. Akselman, M. Vernet, Diversity of the diatom genus *Fragilariopsis* in the Argentine Sea and Antarctic waters: Morphology, distribution and abundance. *Polar Biol.* **33**, 1463–1484 (2010).

73. X. Crosta, O. Romero, L. K. Armand, J.-J. Pichon, The biogeography of major diatom taxa in Southern Ocean sediments: 2. Open ocean related species. *Palaeogeogr. Palaeoclimatol. Palaeoecol.* **223**, 66–92 (2005).

74. S. T. Belt, T. A. Brown, L. Ampel, P. Cabedo-Sanz, K. Fahl, J. J. Kocis, G. Massé, A. Navarro-Rodriguez, J. Ruan, Y. Xu, An inter-laboratory investigation of the Arctic sea ice biomarker proxy IP_{25} in marine sediments: Key outcomes and recommendations. *Clim. Past* **10**, 155–166 (2014).

75. S. T. Belt, P. Cabedo-Sanz, L. Smik, A. Navarro-Rodriguez, S. M. P. Berben, J. Knies, K. Husum, Identification of paleo Arctic winter sea ice limits and the marginal ice zone: Optimised biomarker-based reconstructions of late Quaternary Arctic sea ice. *Earth Planet. Sci. Lett.* **431**, 127–139 (2015).

76. J. J. Brocks, J. M. Hope, Tailing of chromatographic peaks in GC-MS caused by interaction of halogenated solvents with the ion source. *J. Chromatogr. Sci.* **52**, 471–475 (2014).

77. S. T. Belt, W. G. Allard, G. Massé, J.-M. Robert, S. J. Rowland, Highly branched isoprenoids (HBIs): Identification of the most common and abundant sedimentary isomers. *Geochim. Cosmochim. Acta* **64**, 3839–3851 (2000).

78. M. Stuiver, H. A. Polach, Discussion reporting of ^{14}C data. *Radiocarbon* **19**, 355–363 (1977).

79. M. Stuiver, P. J. Reimer, R. W. Reimer, 2022. CALIB 8.2 [WWW program], http://calib.org [accessed 15 March 2022].

80. T. J. Heaton, P. Köhler, M. Butzin, E. Bard, R. W. Reimer, W. E. N. Austin, C. Bronk Ramsey, P. M. Grootes, K. A. Hughen, B. Kromer, P. J. Reimer, J. Adkins, A. Burke, M. S. Cook, J. Olsen, L. C. Skinner, Marine20—The marine radiocarbon age calibration curve (0–55,000 cal BP). *Radiocarbon* **62**, 779–820 (2020).

81. T. J. Heaton, M. Butzin, E. Bard, C. Bronk Ramsey, K. A. Hughen, P. Köhler, P. J. Reimer, Marine radiocarbon calibration in polar regions: A simple approximate approach using Marine20. *Radiocarbon*, 1–28 (2023).

82. M. Paterne, E. Michel, V. Héros, Variability of marine ^{14}C reservoir ages in the Southern Ocean highlighting circulation changes between 1910 and 1950. *Earth Planet. Sci. Lett.* **511**, 99–104 (2019).

83. K. J. Licht, W. L. Cunningham, J. T. Andrews, E. W. Domack, A. E. Jennings, Establishing chronologies from acid-insoluble organic 14C dates on Antarctic (Ross Sea) and Arctic (North Atlantic) marine sediments. *Polar Res.* **17**, 203–216 (1998).

84. J. Haslett, A. Parnell, A simple monotone process with application to radiocarbon-dated depth chronologies. *J. R. Stat. Soc. Ser. C* **57**, 399–418 (2008).

85. H. Goosse, V. Brovkin, T. Fichefet, R Haarsma, P. Huybrechts, J. Jongma, A. Mouchet, F. Selten, P.-Y. Barriat, J.-M. Campin, E. Deleersnijder, E. Driesschaert, H. Goelzer, I. Janssens, M.-F. Loutre, M. A. Morales Maqueda, T. Opsteegh, P.-P. Mathieu, G. Munhoven, E. J. Pettersson, H. Renssen, D. M. Roche, M. Schaeffer, B. Tartinville, A. Timmermann, S. L. Weber, Description of the Earth system model of intermediate complexity LOVECLIM version 1.2. *Geosci. Model Dev.* **3**, 603–633 (2010).

86. A. Berger, Long-term variations of caloric insolation resulting from the earth's orbital elements. *Quatern. Res.* **9**, 139–167 (1978).

87. L. Menviel, E. Capron, A. Govin, A. Dutton, L. Tarasov, A. Abe-Ouchi, R. N. Drysdale, P. L. Gibbard, L. Gregoire, F. He, R. F. Ivanovic, M. Kageyama, K. Kawamura, A. Landais, B. L. Otto-Bliesner, I. Oyabu, P. C. Tzedakis, E. Wolff, X. Zhang, The penultimate deglaciation: Protocol for Paleoclimate Modelling Intercomparison Project (PMIP) phase 4 transient numerical simulations between 140 and 127 ka, version 1.0. *Geosci. Model Dev.* **12**, 3649–3685 (2019).

88. A. Abe-Ouchi, F. Saito, K. Kawamura, M. E. Raymo, J. Okuno, K. Takahashi, H. Blatter, Insolation-driven 100,000-year glacial cycles and hysteresis of ice-sheet volume. *Nature* **500**, 190–193 (2013).

89. P. Köhler, C. Nehrbass-Ahles, J. Schmitt, T. F. Stocker, H. Fischer, A 156 kyr smoothed history of the atmospheric greenhouse gases CO_2, CH_4, and N_2O and their radiative forcing. *Earth Syst. Sci. Data* **9**, 363–387 (2017).

90. F. Fetterer, K. Knowles, W. Meier, M. Savoie, A. K. Windnagel, *Sea Ice Index, Version 3* (NSIDC National Snow Ice Data Center, 2017).

91. A. H. Orsi, T. Whitworth, W. D. Nowlin, On the meridional extent and fronts of the Antarctic Circumpolar Current. *Deep Sea Res.* **42**, 641–673 (1995).

92. R. Schlitzer, Ocean Data View (2017). https://odv.awi.de/ [accessed 6 February 2017].

93. P. U. Clark, A. S. Dyke, J. D. Shakun, A. E. Carlson, J. Clark, B. Wohlfarth, J. X. Mitrovica, S. W. Hostetler, A. Marshall McCabe, The Last Glacial Maximum. *Science* **325**, 710–714 (2009).

94. WAIS Divide Project Members, Precise interpolar phasing of abrupt climate change during the last ice age. *Nature* **520**, 661–665 (2015).

95. C. Buizert, K. M. Cuffey, J. P. Severinghaus, D. Baggenstos, T. J. Fudge, E. J. Steig, B. R. Markle, M. Winstrup, R. H. Rhodes, E. J. Brook, T. A. Sowers, G. D. Clow, H. Cheng, R. L. Edwards, M. Sigl, J. R. McConnell, K. C. Taylor, The WAIS Divide deep ice core WD2014 chronology. Part 1. Methane synchronization (68–31 ka BP) and the gas age–ice age difference. *Clim. Past.* **11**, 153–173 (2015).

96. P. J. Huybers, (2006-08-24): *NOAA/WDS Paleoclimatology–Huybers 2006 Integrated Summer Insolation Forcing Data*. [j_65south.txt]. NOAA National Centers for Environmental Information, https://doi.org/10.25921/nv5w-rh04 [accessed 31 March 2020].

97. J. Laskar, P. Robutel, F. Joutel, M. Gastineau, A. C. M. Correia, B. Levrard, A long-term numerical solution for the insolation quantities of the Earth. *Astron. Astrophys.* **428**, 261–285 (2004).

98. A. D. Moy, M. R. Palmer, W. R. Howard, J. Bijma, M. J. Cooper, E. Calvo, C. Pelejero, M. K. Gagan, T. B. Chalk, Varied contribution of the Southern Ocean to deglacial atmospheric CO_2 rise. *Nat. Geosci.* **12**, 1006–1011 (2019).

99. S. Eggleston, J. Schmitt, B. Bereiter, R. Schneider, H. Fischer, Evolution of the stable carbon isotope composition of atmospheric CO_2 over the last glacial cycle. *Paleoceanography* **31**, 434–452 (2016).

100. J. Lippold, J. Grützner, D. Winter, Y. Lahaye, A. Mangini, M. Christl, Does sedimentary $^{231}Pa/^{230}Th$ from the Bermuda Rise monitor past Atlantic Meridional Overturning Circulation? *Geophys. Res. Lett.* **36**, L12601 (2009).